ACS Catalysis

Research Article

pubs.acs.org/acscatalysis

Effective Strategy for Improving Electrocatalyst Durability by Adhesive Immobilization of Catalyst Nanoparticles on Graphitic Carbon Supports

Albert Epshteyn,*[,†] Yannick Garsany,[‡] Karren L. More,[§] Harry M. Meyer, III,[§] Vaibhav Jain,[†] Andrew P. Purdy,[†] and Karen E. Swider-Lyons[†]

[†]Naval Research Laboratory,Washington, D.C. 20375, United States

[‡]EXCET INC., Springfield, Virginia 22151, United States

[§]Oak Ridge National Laboratory, Oak Ridge, Tennessee 37831, United States

Supporting Information

ABSTRACT: We have found that Ta-based additive films in our catalyst system act as adhesives, which improves electrocatalyst durability by immobilizing the catalyst Pt NPs on the graphitic Vulcan carbon support. Furthermore, we suggest that this can be a general design principle in producing higher-durability electrocatalysts on graphitic supports. By electrochemically probing the contributing roles of the tantalum oxide (Ta_2O_5) and the polyphosphate (PPA) components in separate samples, we show that these combine to produce the observed improvement in activity and durability of our best catalyst, the tantalum polyphosphate ($TaOPO_4$)-treated sample. To control variables for a valid electrochemical comparison, such as dissimilar catalyst particle size distributions and variations in surface coverage, four new catalyst samples closely matched in every way were prepared: (1) Pt/VC, (2) Pt/[PPA/VC], (3) Pt/[Ta_2O_5/VC], and (4) Pt[$TaOPO_4$/VC]. We present HR-TEM/HAADF-STEM, EDS elemental mapping, PXRD, XPS, and electrochemical activity and durability evidence, showing that the $TaOPO_4$ and Ta_2O_5 additives act as adhesives, effectively tethering the NPs to the VC graphitic support surface. Pt/[Ta_2O_5/VC] exhibited 3× better durability as compared with the Pt/VC control because of better catalyst nanoparticle immobilization by the Ta_2O_5 adhesive. Pt[$TaOPO_4$/VC] is the overall best performer, exhibiting both a high MA of 0.82 A mg_{Pt}^{-1}, the highest ORR MA after heat treatment, as well as 1.75× greater durability over the Pt/VC control.

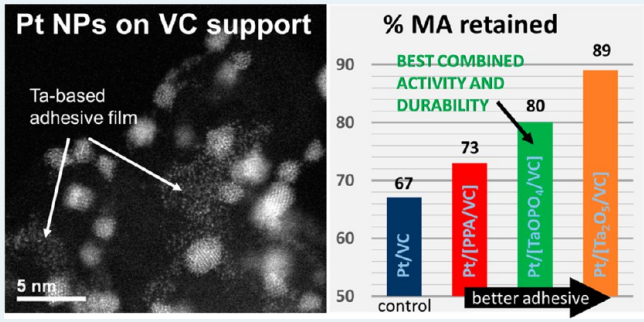

KEYWORDS: *tantalum polyphosphate, nanoglue, anchoring, ORR, durability, nanoparticle ripening*

INTRODUCTION

We present evidence that it is possible to attach Pt catalyst nanoparticles (NPs) to graphitic carbon supports using a cross-linked inorganic adhesive film producing an oxygen reduction reaction (ORR) electrocatalyst with significantly increased durability while maintaining, and even improving, catalytic activity as tested by rotating disk electrode (RDE) measurements. This is a generally significant technological achievement potentially applicable to any NP-based graphitic-carbon-supported electrocatalyst. Degradation of heterogeneous catalysts via catalyst particle ripening is a problem that has been extensively studied for many catalyst systems and generally resolved by catalyst particle anchoring as well as particle encapsulation on oxide supports.[1] However, it is a particularly challenging problem to anchor catalyst particles on conductive graphitic supports for electrocatalyst applications.[2] Our approach is therefore to not attempt to derivatize the surface, as is done with oxide supports, but rather, to deposit a weblike Ta-based inorganic film on all nanocomposite catalyst support surfaces, thereby "gluing" the components together with significantly less than a monolayer of the Ta-based adhesive that does not interfere with the ORR while successfully immobilizing the Pt catalyst NPs.

The ubiquitous use of polymer electrolyte membrane fuel cells (PEMFCs) for portable and transportation applications is currently not economically viable, in part because of the costs associated with the use of platinum-based ORR catalysts employed in PEMFCs.[2] A commercially attractive ORR catalyst would be a significant technological achievement, and not only must it be highly active to justify its materials costs, but also its activity must not degrade in the corrosive environment of the PEMFC cathode because its durability directly impacts the FC performance and maintenance costs.[2,3] The experimentally observable manifestation of ORR catalyst aging is a measured

Received: November 11, 2014
Revised: April 28, 2015
Published: May 18, 2015

DOI: 10.1021/cs501791z
ACS Catal. 2015, 5, 3662−3674

loss in the electrochemically active surface area (ECSA), which directly affects the total catalyst mass activity (MA), adversely impacting the power output of the fuel cell. The highly corrosive cathode environment includes a high proton concentration in combination with the cell potential. Even relatively inert materials, such as graphitic carbon and Pt, corrode under these conditions; in particular, the degradation of Pt ORR catalysts has been shown to proceed via a set of well-defined, albeit not fully understood, mechanisms.[2−4] Specifically, (1) platinum dissolution and redeposition, (2) particle migration and coalescence, (3) particle detachment, and (4) corrosion of the carbon support itself are the generally accepted degradation pathways, with evidence pointing to all of these modes contributing to the catalyst aging process to some extent.[3a,4b,5]

Designing an ORR catalyst that is more stable against aging and degradation while at the same time maintaining a high catalytic activity is a formidable technological barrier preventing PEMFCs from being more economically viable. Hence, the focus of the work presented herein is on how adhesive immobilization can improve ORR catalyst durability by eliminating particle migration and coalescence. We propose that this adhesive immobilization of catalyst NPs not only is useful for PEMFC applications but also is generally applicable to other electrocatalyst systems requiring conductive graphitic carbon catalyst supports.

There has been much interest in the PEMFC community directed at the ORR catalyst degradation mechanism producing compelling studies of degradation phenomena under voltage cycling, with reports of morphological characterization by atomic force microscopy (AFM), identical location transmission electron microscopy (IL-TEM), and in situ TEM, as well as IL-TEM-coupled IL-electron energy loss spectroscopy (EELS) tomography, producing the most direct evidence to date that coalescence of neighboring particles is in large part responsible for catalyst particle growth and overall catalyst degradation.[5,6]

In response to this growing body of mechanistic evidence, there have been numerous recent reports showing that restriction or elimination of catalyst particle movement in various electrocatalysts improves catalyst durability. For example, Galeano, Meier, and co-workers report that Pt NPs encapsulated in mesoporous graphitic spheres are significantly more stable as compared with Pt NPs dispersed directly onto Vulcan carbon (VC).[7] Pylypenko et al. present evidence that nitrogen-doped graphitic carbon stabilizes Pt alloy NPs by preventing particle growth due to the NPs adhering stronger to nitrogen-rich support surface regions that limit particle mobility.[8] Ionic liquids and hydrophobic silica have also been shown to stabilize Pt nanoparticles on single-walled carbon nanotubes, increasing catalyst durability.[9] In another recent report, Chen, Wei, and co-workers have shown a benefit for catalyst durability after coating the carbon support with a conductive polyaniline polymer achieved by polymerizing the monomer on the support surface following the introduction of the Pt NPs.[10] It has also been suggested that the use of a graphene oxide surface to first anchor catalyst particles, followed by the selective reduction of the unoccupied graphene surface restoring (at least partially) support electrical conductivity, may be an approach to immobilizing catalyst particles on a hybrid graphene/graphene oxide surface.[11]

We previously reported on the first-generation, highly active and durable ORR catalyst comprising Pt NPs on a tantalum polyphosphate ($TaOPO_4$)-treated VC support, that in rotating disk electrode (RDE) experiments exhibited a mass activity (MA) of 0.46 $A{\cdot}mg_{Pt}^{-1}$ as measured at E = 0.90 V vs a reversible hydrogen electrode (RHE) and more than 2× greater stability to oxidative electrochemical cycling than the 20% Pt E-TEK and Johnson Matthey commercial carbon-supported Pt catalysts.[12] The highly dispersed film of Ta atoms appears as bright dots surrounding the Pt NPs on the VC support, as can be seen in the high-angle annular dark field scanning TEM (HAADF-STEM) image in Figure 1. Only the Pt and Ta are

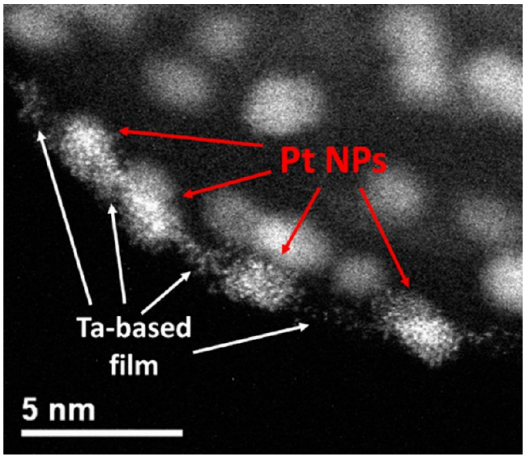

Figure 1. HAADF-STEM image of original 18 wt % Pt on $TaOPO_4$ treated VC. In the image, VC support is decorated with Pt NPs that are "glued" to the VC support by a film containing Ta atoms, with the Z-contrast-resolved individual Ta atoms appearing as white dots between the Pt particles.

visible in the image, since the P and O atoms do not provide sufficient Z contrast over the C support. As a complement to the HAADF-STEM, direct observation of the Pt and Ta atoms on the VC surface, energy-dispersive X-ray spectroscopy (EDS) elemental mapping (Figure S1) provides convincing evidence for the colocation of Pt, Ta, P, and O atoms in the sample. It is this microstructure that at the same time enables contact between the $TaOPO_4$ film, the Pt particles, and the VC surface without separating the Pt from the current collector or blocking Pt active sites and ultimately provides facile reactant and product diffusion. Note that all of the Pt NPs are associated with the Ta-based film.

An added benefit of the synthesis method we have employed, whereby presynthesized colloid-derived Pt NPs are cast and attached onto VC supports, is the highly homogeneous distribution of the uniformly sized Pt particles on the VC support surface, which is known to be of significant importance for high-activity catalysts, as well as providing a well-defined and tunable catalyst system for study.[13] This highly uniform, well-defined, and reproducible catalyst system presents a unique opportunity to make the direct comparison between catalysts by varying the adhesive additive component while eliminating the possibility of other variables influencing the system.[13]

Herein, we explore the role of the Ta-based film and its components for the observed improvement in voltage cycling durability. We conclude that although there may be other variables, the main characteristic of the film imparting the observed improvement in durability is the immobilization of the Pt catalyst particles. We present evidence of the attachment

DOI: 10.1021/cs501791z
ACS Catal. 2015, 5, 3662−3674

of the Pt NPs to the VC support surface and correlate this observation with the catalyst durability performance. For the purposes of this study, we examine the performance of the polyphosphoric acid (PPA) and the tantalum oxide (Ta_2O_5) adhesive components, alongside the previously reported tantalum polyphosphate ($TaOPO_4$), to better understand the observed improvements in durability for this catalyst system.

To that end, we prepared a set of new, 10 wt % Pt catalysts on VC support in the same manner as the original $TaOPO_4$-treated catalyst. The treatments consisted of the separate adhesive components of PPA (for the PPA-treated sample) and also $Ta(OE)_5$ + H_2O (for the Ta_2O_5 treated sample), to discriminate between the roles of each component in imparting improved durability, thereby correlating the composition and morphology of each sample with observed ORR activity after voltage cycling. XPS data reveal that during heat treatment, a significant portion of the Ta_2O_5 is reduced to a Ta-suboxide, which may explain its lower ORR activity. There is a particularly strong detrimental impact to its specific activity (SA), which eclipses its superior durability. On the other hand, on the basis of the X-ray photoelectron spectroscopy (XPS) results, the $TaOPO_4$-treated sample is stable to heat treatment, resulting in significantly higher ORR activity. The $TaOPO_4$ sample appears to be a good compromise because it combines the benefits of both the higher SA (as in the presence of PPA) and the durability of the robust Ta oxide film components.

EXPERIMENTAL SECTION

As previously reported, the Pt colloid was synthesized via a literature procedure from Wang et al.[14] that was modified to a larger-scale synthesis (4 L, ∼ 10 g Pt), which produced small and monodisperse Pt NPs on the order of 1.7 nm average diameter with a narrow size distribution.[12] The nanoscale Pt/[$TaOPO_4$/VC] was synthesized from $Ta(OEt)_5$ and PPA mixed with VC and the subsequent addition of colloid-derived Pt NPs, as described in our prior work.[12,15] The synthesis of the Pt/[Ta_2O_5/VC] is a variation on the same method in which the VC was suspended in ethanol (EtOH) and mixed with $Ta(OEt)_5$ in EtOH and sonicated for 2 h. A stoichiometric amount (with respect to Ta) of Nanopure water was then added to the reaction, and it was sonicated overnight. The same colloid-derived Pt NPs were deposited on the tantalum oxide-coated VC in the same manner as for the Pt/[$TaOPO_4$/VC]. The resulting materials were heat-treated in a tube furnace under a flow of ultrahigh purity (UHP) Ar (99.9995% Airliquid) with an initial ramp of 10 °C/min to 660 °C, followed by a 2 h hold at 660 °C, then followed by passive cooling to ambient temperature still under a flow of UHP Ar.

The Pt content for each of the electrocatalysts was determined by ICP-OES using a PerkinElmer Optima 2000 DV ICP-OES analysis of solutions obtained by a single dilution of 5% HF in aqua regia digests of the electrocatalyst samples, which were digested at room temperature for 3 days before the analyses were performed. The analyses were validated by determining the Pt content of known commercial Pt/VC electrocatalysts (19.7 wt % Pt, E-TEK, 40 wt % Pt, Johnson-Matthey HiSPEC 4000). The Ta content was estimated by XPS to be near 0.6−0.8 at. % for those samples that contain Ta (see Table S1), which is in line with 3 wt % previously reported for 18% Pt/[$TaOPO_4$/VC]-HT as determined by wet chemical analysis.[12] Electrochemical ORR activity and durability testing were performed using previously reported standard procedures and are described in detail in the Supporting Information.[12,16]

Powder X-ray diffraction (PXRD) was performed on a Rigaku SmartLab diffractometer equipped with a Cu source and a DteX linear detector. XPS analyses were performed on a Thermo K-Alpha system after the powder samples were pressed into indium foil (Aldrich, 99.999 %). Survey scans and core level spectra were obtained using pass energies of 100 and 50 eV, respectively. All XPS data were corrected for electrostatic charging using the XPS lines of C (1s) as the internal reference energy. Scanning transmission electron microscopy (STEM) imaging was performed on a probe-corrected JEOL 2200 FS TEM/STEM equipped with a Bruker X-flash 30 mm^2 silicon drift detector for acquisition of energy dispersive X-ray spectroscopy (EDS) data and elemental maps. Other high resolution (HR)-TEM imaging was performed at 200 keV on a JEOL 2010F equipped with a field emission gun (FEG). The particle size distribution statistics were determined from the evaluation of the HR-TEM and HAADF-STEM images by measuring the diameter of at least 200 particles for each sample.

RESULTS AND DISCUSSION

Nanocomposite Electrocatalyst Preparation and Characterization. *Resistance against Particle Growth during Heat Treatment.* Electrochemical testing of the previously reported 18 wt % Pt/[$TaOPO_4$/VC] showed that the catalyst initially isolated after low-temperature drying (i.e., 40 °C in a vacuum oven) had impaired ORR activity.[12] We found that heat treatment under inert atmosphere rectified the problem. During our heat treatment study, we found that heating the original 18 wt % Pt/[$TaOPO_4$/VC] sample to between 150 and 250 °C (even for several days) was insufficient to produce Pt crystallites any larger than 1.8 nm; furthermore, the Pt crystallites in the $TaOPO_4$-treated sample did not grow larger than 1.8 nm until exposure to temperatures in the 600−800 °C range. The stacked diffractograms of the 18 wt % Pt/[$TaOPO_4$/VC] sample heated to progressively higher temperatures in the 400−800 °C range in Figure 2 are illustrative of the resistance to sintering imparted by the $TaOPO_4$ additive. In comparison, the control 18 wt % Pt/VC sample without any adhesive additives grew to 2.4 nm after heating to 150 °C for 2 h (Figure S2). This phenomenon is illustrative of the stabilization against sintering that the $TaOPO_4$ adhesive imparts on the Pt NPs dispersed on the VC surface. RDE testing of these catalysts showed the highest activity for the sample heated to 650 °C.[12]

The Pt NP size distribution data from particle diameter measurements in HR-TEM before and after heat treatment for the original 18 wt % Pt/[$TaOPO_4$/VC] sample reveals further evidence of the immobilization of Pt particles on the VC surface (Figure 3). The particle size distribution before heating appears to exhibit a natural Poisson shape with a mean diameter of 1.6 nm (Figure 3a), as would be expected from the as-synthesized colloid-derived Pt NPs; whereas the same sample heated to 650 °C for 2 h exhibits three distribution maxima at 2.0, 2.4, and 3.0 nm (Figure 3b). This trimodal particle size distribution is observable only as a result of the highly monodisperse particle size distribution of the original colloid. The trimodal particle size distribution produced after heating indicates that coalescence takes place only for those particles that are deposited close enough to each other to coalesce, as controlled by particle loading in turn affecting average interparticle distance, hence producing the observed trimodal distribution in Figure 3b. It is possible to imagine that the distribution with the maximum at 2.4 nm is the result of

DOI: 10.1021/cs501791z
ACS Catal. 2015, 5, 3662−3674

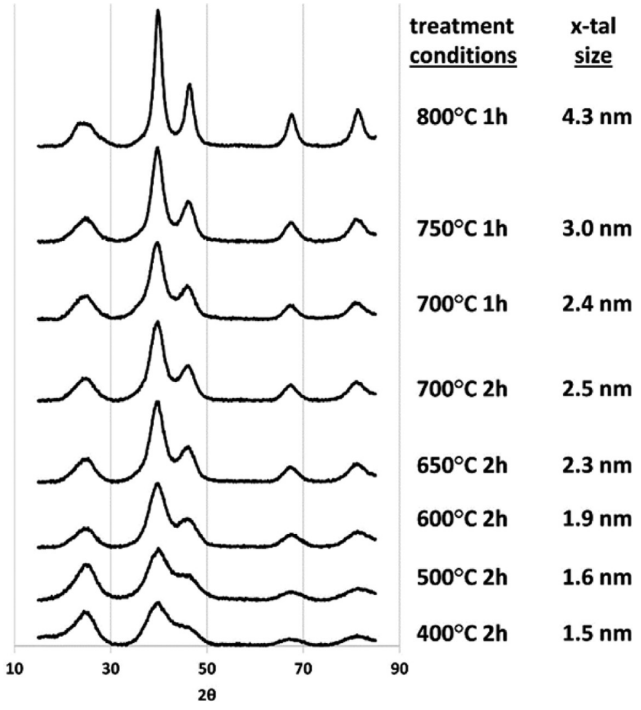

Figure 2. PXRD diffractograms of 18% Pt/[$TaOPO_4$/VC] nanocomposite samples heated in the temperature range from 400 to 800 °C under an Ar atmosphere and the corresponding Scherrer Pt crystallite diameter.

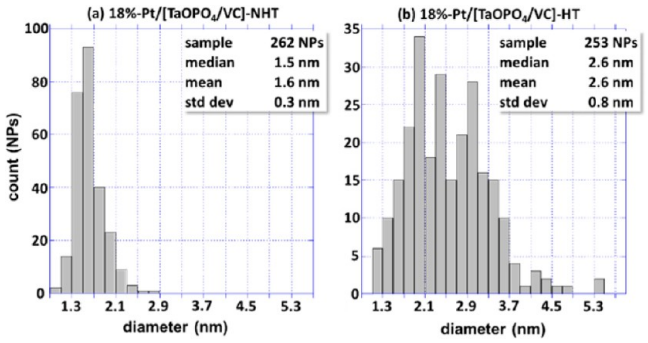

Figure 3. HR-TEM-derived particle diameter statistics: (a): particle size distribution for 18% Pt/[TaOPO4/VC]-NHT; (b): Pt particle size distribution for 18 wt % Pt/[$TaOPO_4$/VC]-HT.

those instances when two neighboring particles coalesced, and the distribution with a maximum at 3.0 nm is the result of three neighboring particles coalescing. The distribution with a maximum at 2.0 nm is the slightly shifted original size distribution of those particles that did not coalesce. The particle growth observed in the original 18 wt % Pt loading sample is therefore statistically driven by the likelihood of two or three Pt particles residing on the VC surface in sufficiently close proximity to one-another to coalesce after gaining the necessary mobility at the anneal temperature.

One of our goals in developing this catalyst system with colloid-derived Pt NPs was to make a standard, reproducible, test-bed catalyst, enabling the control of all variables, thereby allowing direct catalyst comparisons. To make deductions regarding the differences observed for various samples, it is necessary to control variables such as Pt loading, particle size distribution, and variations in pretreatment, such as anneal temperature. Because our most active catalyst containing the $TaOPO_4$ additive requires heat treatment, it is problematic that different adhesive additives can affect particle growth during heat treatment to varying degrees. Considering it is the very adhesive nature of the various additives that we wish to probe to study the effect the additives have on the electrocatalyst performance, we set out to prepare a new set of catalysts with a lower Pt loading, thereby increasing the average interparticle distance to minimize particle growth during heat treatment, which makes a direct comparison of activities and durabilities for catalysts with different additives possible.

Synthesis of a New Series of Electrocatalysts. To study and differentiate the effects of each component of the $TaOPO_4$ adhesive on the overall catalyst performance, we designed a new set of electrocatalysts with lower Pt loading that were prepared in the same manner as previously reported by depositing presynthesized Pt colloid onto VC supports, but treated with different additives, as described in the Experimental section.[12,15,17] The amount of Pt in each sample was reduced to 10 wt %, thereby decreasing the probability of particle coalescence during heat treatments and keeping the particle population more homogeneous and monodisperse across all samples after heat treatment. The new samples prepared for this study are (1) a 10 wt % Pt on VC as our control, designated as Pt/VC; (2) a 10 wt % Pt on PPA-treated VC, designated as Pt/[PPA/VC]; (3) a 10 wt % Pt on Ta_2O_5-treated VC, designated as Pt/[Ta_2O_5/VC]; and (4) a 10 wt % Pt sample prepared with $TaOPO_4$ in the same manner as the originally reported electrocatalyst, designated as Pt/[$TaOPO_4$/VC]. For Pt/[PPA/VC], the PPA was introduced alone without the addition of $Ta(OEt)_5$. For the Pt/[Ta_2O_5/VC] sample, the $Ta(OEt)_5$ was introduced with a stoichiometric amount of water to produce a Ta_2O_5 precursor that upon heating forms the Ta_2O_5 film comparable to the film observed for $TaOPO_4$. Samples before heat treatment are designated NHT (not heat treated) and HT after heat treatment.

Compositional and Morphological Characterization of the New Electrocatalysts. Scherrer analyses of the PXRD patterns from all four 10 wt % Pt samples after heat treatment (Figure S3), confirm that the new, lower Pt content catalysts do not grow as much as the original 18 wt % Pt sample. In fact, the 10 wt % loading was sufficiently low to significantly reduce particle coarsening for all four samples, including the Pt/VC control that did not contain adhesive additives. Although the observed differences are close to, or even within the margin of error of, the four samples, the $TaOPO_4$-treated sample grew the least, with its average crystallite size remaining near 1.8 nm. This crystallite diameter is roughly the same as the original particle diameter for the Pt colloid. The other three samples grew slightly larger in comparison, with the average particle diameter increasing to ~2 nm. On the basis of the PXRD data, all four samples have a similar average Pt crystallite diameter after heat treatment, which was the specific goal for a valid direct activity and durability comparison between these samples.

Because the PXRD data provide only the average Pt crystallite size that is biased against crystallites smaller than 1 nm in diameter, TEM/STEM were employed as a complementary technique to obtain accurate statistical Pt catalyst particle population size data as well as to examine the morphology of the catalysts and verify that the Pt NPs were distributed homogeneously on the VC surface. A comparison of HAADF-STEM images of the four electrocatalyst samples in

DOI: 10.1021/cs501791z
ACS Catal. 2015, 5, 3662−3674

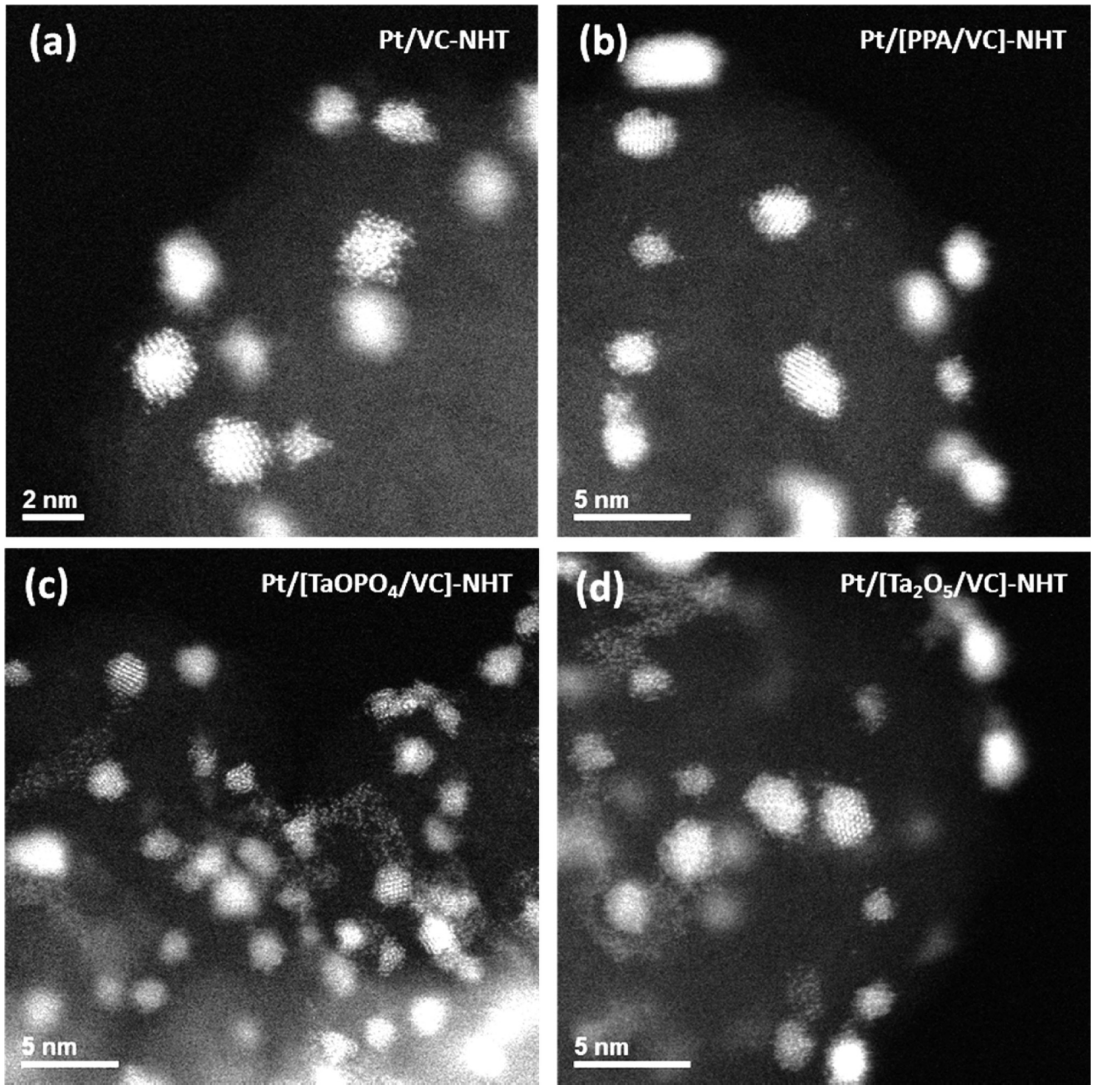

Figure 4. HAADF-STEM images of (a) Pt/VC-NHT; (b) Pt/[PP/VC]-NHT; (c) Pt/[$TaOPO_4$/VC]-NHT; and (d) Pt[Ta_2O_5/VC]-NHT samples, showing the uniform nearly identical morphologies for all four samples, with the main visible difference being the presence of films of Ta atoms between the Pt particles in images c and d.

Figure 4 confirms that all four samples have similar Pt particle sizes and exhibit good particle dispersions across the VC surface, with the main difference between the samples being the presence of Ta atoms visible by the *Z*-contrast imaging in Figure 4c and d, but not present in a and b. Also noteworthy is the colocation of the Pt NPs with the visible areas of Ta atoms for the Pt/[$TaOPO_4$/VC] and Pt/[Ta_2O_5/VC] samples, which along with the EDS elemental maps (Figure S1) support that the Pt NPs are associated with the Ta-based films.

Images a and b in Figure 5, which are a HR-TEM bright field image and HAADF-STEM image, respectively, from an identical area of the Pt/[$TaOPO_4$/VC]-NHT sample, illustrate how *Z*-contrast (HAADF-STEM) imaging provides direct visualization of the high-*Z* Ta and Pt atoms. In image b, a HAADF-STEM image, rivers of Ta atoms are evident as low-density, yet generally continuous, films on the VC surface between the Pt particles. A further examination of the samples in images c and d in Figure 5, which are of the Pt/[$TaOPO_4$/VC] sample before and after heat treatment, respectively, reveals a uniform Pt particle distribution on the VC surface, with few Pt particles in direct contact with each other and few changes occurring after heat treatment. The exemplar HAADF-STEM images of the Pt/[$TaOPO_4$/VC] sample in Figure 5b–f provide compelling evidence that the Pt particles are associated with the Ta-based film before and after heat treatment. Images c, d, e, and f in Figure 5 are HAADF-STEM images of the Pt/[$TaOPO_4$/VC] sample before and after heat treatment, showing that the Ta-based film on the VC surface remains intact after heating, and the crystallization of the Pt NPs observed by PXRD is further supported by the improved definition of truncated cuboctahedral particle edges and the overall more spherical morphology of the Pt particles in the heated sample in d and f, as compared with the more disordered edges of the Pt particles and qualitatively more elongated shape of the Pt particles in the unannealed sample in c and e.

A detailed analysis of Pt particle size distributions based on statistically significant particle population samples of at least 200 particles for each sample was conducted for the samples before and after heat treatment using images acquired via both TEM (Figure S6) and HAADF-STEM (Figure S7), with the Pt particle size data summarized in Figure 6. According to the

DOI: 10.1021/cs501791z
ACS Catal. 2015, 5, 3662–3674

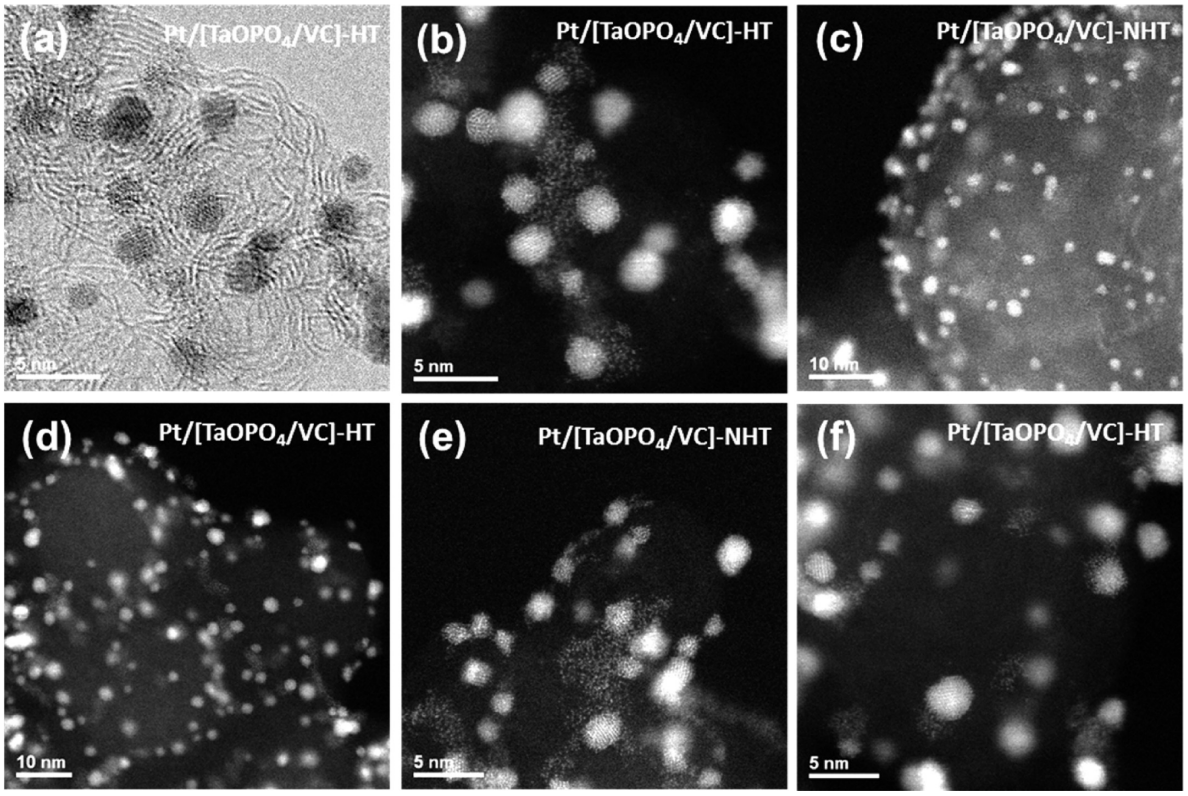

Figure 5. STEM images of Pt/[$TaOPO_4$/VC]: (a) bright field STEM image of Pt/[$TaOPO_4$/VC]-NHT; (b) HAADF-STEM of the same area as panel a; (c) image of Pt/[$TaOPO_4$/VC]-NHT showing the homogeneous distribution of Pt particles on VC support surface; (d) image of Pt/[$TaOPO_4$/VC]-HT showing that the homogeneous distribution of Pt particles on the VC support surface remains after heat treatment; (e) image of Pt/[$TaOPO_4$/VC]-NHT showing Pt particles with irregular edges as well as the Ta atoms forming a film on the VC surface; (f) image of Pt/[$TaOPO_4$/VC]-HT showing the Pt particles now have a more defined cuboctahedral shape with sharper edges defining the Pt particles, as well as the intact $TaOPO_4$ film on the VC surface between the Pt particles.

particle sizing statistics, after heat treatment, the mean particle diameter for Pt/VC increased from 1.7 to 2.1 nm (Figure 6a,b); for Pt/[PPA/VC], the mean diameter increased from 1.6 to 2.0 nm (Figure 6c,d); for Pt/[$TaOPO_4$/VC], the mean diameter remained at 1.8 nm (Figure 6e,f); and for Pt/[Ta_2O_5/VC], the mean diameter increased from 1.7 to 2.0 nm (Figure 6g,h), further confirming the successful synthesis of samples that have similar particle sizes and statistically similar particle size distributions, allowing for a direct comparison of catalyst electrochemical activity and durability in the presence or absence of additives. The TEM-derived Pt particle size distributions correlate well with the average Pt crystallite size as determined by Scherrer analysis of PXRD peaks for each of the heated samples summarized in Table 1.

XPS analyses were performed on the four new catalyst samples to confirm the presence of additives introduced during the synthesis, with the survey spectra for the analyzed samples shown in Supporting Information Figure S8; the surface atomic composition determined from XPS data can be found in Supporting Information Table S1. XPS confirmed that Ta was not present in the Pt/VC and Pt/[PPA/VC] samples. The Pt/[PPA/VC] sample showed a small amount of P present at the same level as S, which is known to be present in VC at ~5000 ppm.[18] Samples Pt/[$TaOPO_4$/VC]-NHT and Pt/[$TaOPO_4$/VC]-HT showed the highest amount of P at ~1.2 at. %. The Pt/[$TaOPO_4$/VC] and Pt/[Ta_2O_5/VC] samples showed about the same amount of Ta, ~0.6−0.8 at. %, which is similar to our previously reported 3 wt % Ta for the 18 wt % Pt/[$TaOPO_4$/VC].[12] Samples Pt/VC, Pt/[Ta_2O_5/VC]-NHT, and Pt/[Ta_2O_5/VC]-HT showed no P, as expected. The XPS data confirm that the appropriate additives were, indeed, delivered to produce the four intended catalyst samples.

Most of the XPS data were consistent with expected catalyst compositions and are shown in Supporting Information Figures S9−S16; however, closer analysis of the Ta core level spectra (Figure 7) for the Pt/[$TaOPO_4$/VC] and Pt/[Ta_2O_5/VC] before and after heat treatment provided interesting insight that is possibly relevant to explain the observed differences in ORR catalytic activity between these samples. The Ta 4f doublets for both samples before heating are nearly identical, with the Pt/[$TaOPO_4$/VC]-NHT binding energy (BE) of 26.34 eV for the 7/2 peak and 28.29 eV for the 5/2 peak and the Pt/[Ta_2O_5/VC]-NHT BE of 26.35 eV for the 7/2 peak and 28.30 eV for the 5/2 peak, which are consistent with the expected Ta^{5+} signal from Ta_2O_5.[19] In the heated samples, however, there is a significant difference. Although the Pt/[$TaOPO_4$/VC] sample appears to be almost entirely stable during the heat treatment, with only 2.7% of the Ta reduced to a new species showing a 4f 7/2 signal at 23.76 eV, there are two new Ta 4f doublets for Pt/[Ta_2O_5/VC] after heat treatment, one of which appears to be the same as the minor species appearing after heat treament for the Pt/[$TaOPO_4$/VC] sample with the 7/2 peak at 23.85 eV, in the case of Pt/[Ta_2O_5/VC] accounting for 7.4% of Ta, and another new, less reduced species with the 7/2 peak appearing at 25.55 eV accounting for a very significant 55.4% of the Ta signal. These new peaks are reduced Ta suboxides, which are probably forming at elevated temperatures as a result of the proximity of Pt and VC, and based on the XPS, it appears that

DOI: 10.1021/cs501791z
ACS Catal. 2015, 5, 3662−3674

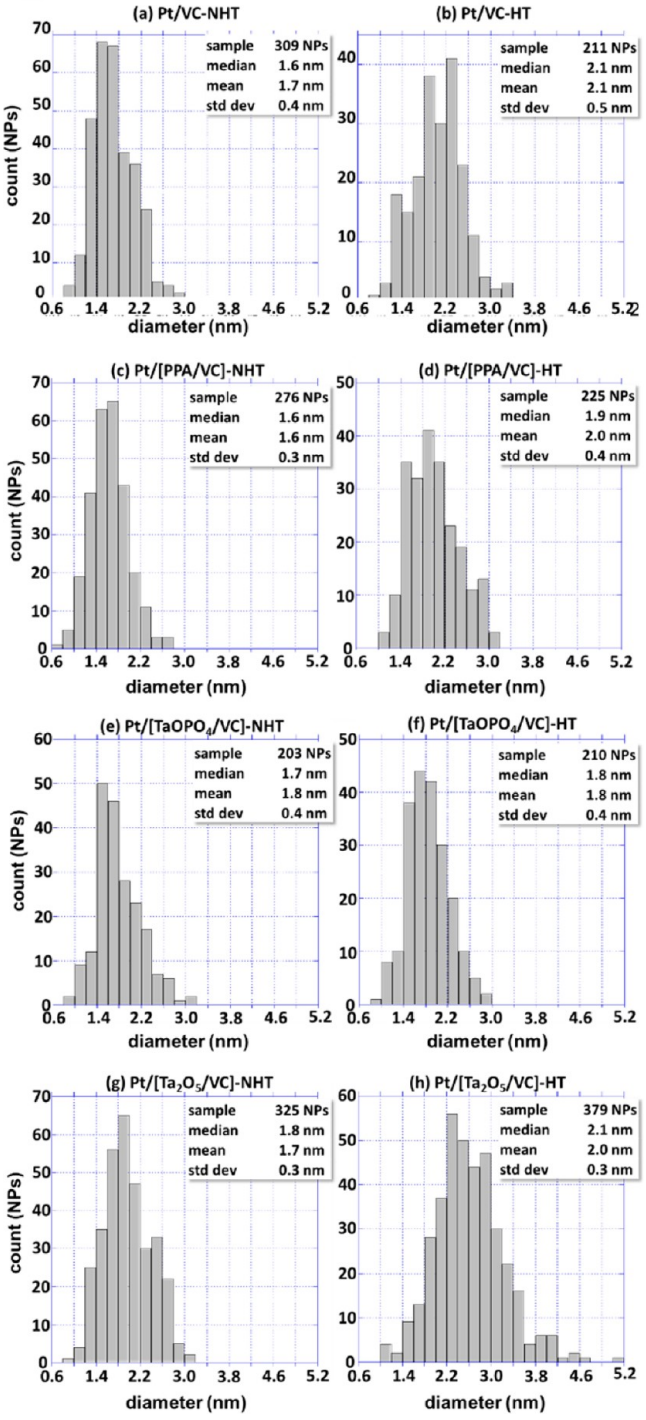

Figure 6. TEM/STEM particle size distributions for each of the electrocatalyst samples before ((a) Pt/VC-NHT, (c) Pt/[PPA/VC]-NHT, (e) Pt/[$TaOPO_4$/VC]-NHT, (g) Pt[Ta_2O_5/VC]-NHT) and after ((b) Pt/VC-HT, (d) Pt/[PPA/VC]-HT, (f) Pt/[$TaOPO_4$/VC]-HT, (h) Pt[Ta_2O_5/VC]-HT) heat treatment.

>62% of the Ta in the Pt/[Ta_2O_5/VC] sample is reduced. On the basis of the match with known Ta-oxide signals and little or no change in the Pt XPS signals of the two samples, we conclude that the Ta is not likely reacting to form an intermetallic species with Pt, as was reported by Gregoire and co-workers;[20] rather, the Ta_2O_5 is reduced. This observed instability and formation of new suboxide species is of significance because the Pt/[Ta_2O_5/VC] sample exhibits much lower SA than the Pt/[$TaOPO_4$/VC] sample, which is discussed in the Electrochemical Catalyst Characterization by RDE section below.

Table 1. Summary of Pt Content As Determined by ICP-OES of Aqua Regia Digests of Each Sample and Respective Particle Sizes As Determined by TEM Particle Size Statistics and PXRD Crystallite Diameters Determined by the Scherrer Method

catalyst sample	Pt loading (wt %)	TEM particle diameter (nm)	PXRD Scherrer diameter (nm)
Pt/VC-NHT	10.64	1.7	
Pt/VC-HT	10.39	2.1	2.0
Pt/[PPA/VC]-NHT	11.42	1.6	
Pt/[PPA/VC]-HT	10.33	2.0	1.9
Pt/[$TaOPO_4$/VC]-NHT	9.53	1.8	
Pt/[$TaOPO_4$/VC]-HT	10.36	1.8	1.7
Pt/[Ta_2O_5/VC]-NHT	9.53	1.7	
Pt/[Ta_2O_5/VC]-HT	10.65	2.0	2.1

In summary, on the basis of the material and morphological characterization of our catalyst samples, we have confirmed that our synthetic approach of lowering the Pt content to 10 wt % for the four new catalyst samples was successful in producing samples with an almost identical Pt particle size, narrow particle size distributions, and good particle dispersion on the VC surface, making possible a direct electrochemical comparison of the samples with any differences in overall catalyst durability attributable to the presence or absence of the PPA, $TaOPO_4$, and Ta_2O_5 additives among the four samples.

Electrochemical Catalyst Characterization by RDE. For the initial comparison to observe electrocatalyst water activation behavior, Figure 8 compares representative cyclic voltammograms (CVs) recorded for the non-heat-treated Pt/VC control, Pt/[PPA/VC], Pt/[$TaOPO_4$/VC], and Pt/[Ta_2O_5/VC] to the CVs recorded for the same samples that were heat-treated. The CVs were measured in N_2-purged 0.10 M $HClO_4$ aqueous electrolyte at a potential scan rate of 20 mV s^{-1}. The current is normalized to the RDE electrode Pt mass because the Pt loading on the electrode varied between 13 and 18 μg_{Pt} cm^{-2} sample-to-sample. The CVs recorded for the pre- and post-heat-treated Pt/[PPA/VC], Pt/[$TaOPO_4$/VC], and Pt/[Ta_2O_5/VC] electrocatalysts are very similar to the CV recorded for the Pt/VC-NHT standard. In the potential range between 0.05 and 0.40 V vs RHE, the samples exhibit the characteristic hydrogen adsorption and desorption peaks of nanoscale Pt. The hydrogen adsorption/desorption region is followed by the double-layer potential region at 0.40 V $\leq E \leq$0.70 V and the Pt−OH adsorption/reduction potential region at 0.70 V $\leq E \leq$ 1.20 V, which is in good agreement with previous studies.[21] The peaks between 0.1 and 0.2 V and the broad shoulder between 0.2 and 0.3 V correspond to the Pt−H adsorption/desorption on Pt (110) and Pt (100) facets, respectively. It should be noted that all the heat-treated electrocatalysts exhibit lower current in the hydrogen adsorption/desorption region, indicative of a smaller Pt ECSA and an increase in the Pt particle size due to the heat-treatment.

DOI: 10.1021/cs501791z
ACS Catal. 2015, 5, 3662−3674

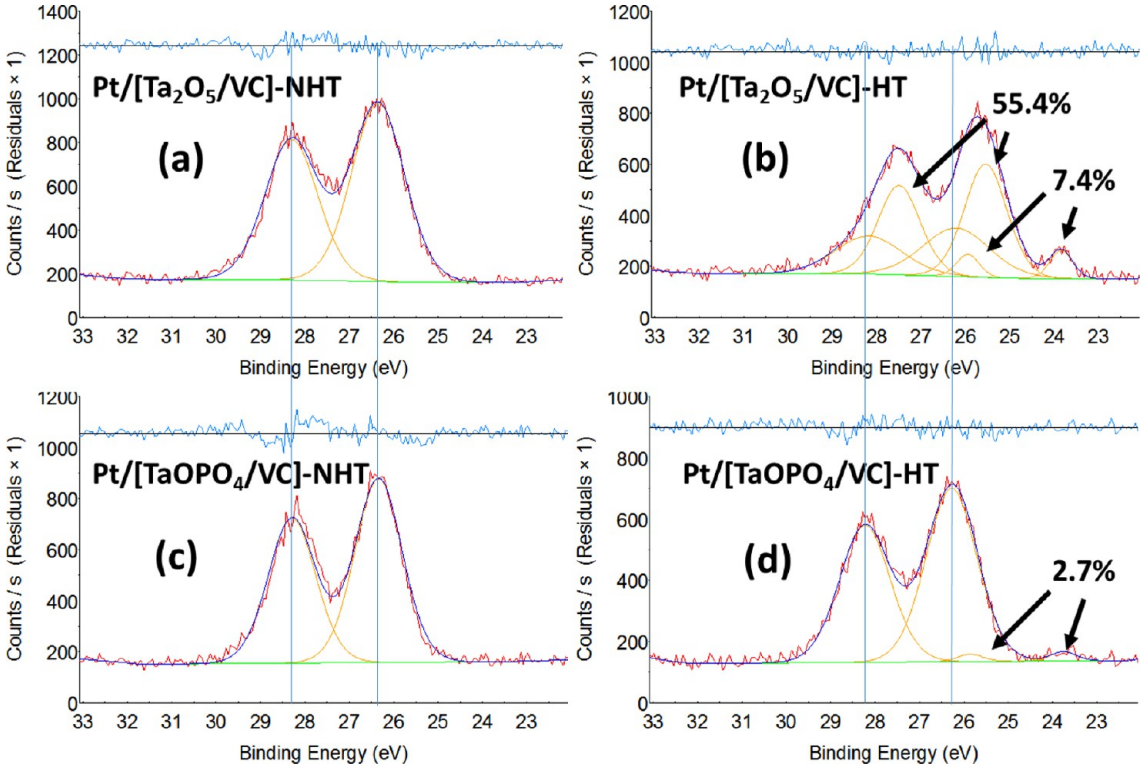

Figure 7. XPS core level spectra of Ta 4f lines for samples (a) Pt/[Ta_2O_5/VC]-NHT, (b) Pt/[Ta_2O_5/VC]-HT, (c) Pt/[$TaOPO_4$/VC]-NHT, and (d) Pt/[$TaOPO_4$/VC]-HT.

Representative *iR* and background corrected ORR polarization curves for the NHT and HT Pt/VC control, Pt/[PPA/VC], Pt/[$TaOPO_4$/VC], and Pt/[Ta_2O_5/VC] electrocatalysts are shown in Figure 9. The ORR polarization curves, which were measured in O_2-saturated 0.10 M $HClO_4$ electrolyte at 30 °C, at an electrode rotation rate of 1600 rpm and potential scan rate of 20 mV s^{-1} (anodic sweep: 0.05 → 1.03 V vs RHE) show a diffusion-controlled region at a potential lower than 0.60–0.75 V with a well-defined limiting current plateau, a diffusion-kinetic combined region, and a kinetically controlled region at a potential ≥0.925 V vs RHE. The same diffusion-limited current density plateau of −6 mA cm^{-2}_{geo} is achieved for all of the electrocatalysts, which is within 5% of the expected limiting current density of the ORR in 0.10 M $HClO_4$ at 1600 rpm (6.02 mA cm^{-2}_{disk}), as shown in Figure 9, indicating a complete 4 e^- reduction process.[22]

The electrocatalyst ORR activity can be visually benchmarked from the half-wave potential, $E_{1/2}$, which is halfway between the zero current and the well-defined limiting current plateau. The measured $E_{1/2}$ for the NHT and HT Pt/VC control are 0.914 and 0.911 V, respectively. The measured $E_{1/2}$ for the NHT and the HT Pt/[PPA/VC] are 0.925 and 0.915 V, respectively. The measured $E_{1/2}$ for the non-heat-treated and the heat-treated Pt/[$TaOPO_4$/VC] are 0.905 and 0.922 V, respectively. The measured $E_{1/2}$ for the NHT and the HT Pt/[Ta_2O_5/VC] are 0.910 and 0.922 V, respectively. The trend in the measured $E_{1/2}$ indicates that the HT Pt/VC control and Pt/[PPA/VC] catalysts, which lack an adhesive Ta-based film immobilizing the Pt particles on the VC surface, are less active than before heat treatment, and the HT Pt/[$TaOPO_4$/VC] and Pt/[Ta_2O_5/VC] catalysts, which do contain Ta-based adhesive films, are more active than they were before heat treatment.

Because the Pt loading on the RDE electrode is not exactly the same for each of the tested electrocatalysts, a valid comparison of the ORR activity cannot be based only on the ORR polarization curves and half-wave potentials. The ORR catalytic activity of the electrocatalysts is best compared by their MA and SA using the mass-transport correction for thin-film RDEs (eq 1),[16c] where I_k is the mass-transport corrected kinetic current and I_{lim} is the limiting current,

$$I_k = \frac{I_{lim} \times I}{I_{lim} - I} \quad (1)$$

measured at E = 0.50 V vs RHE, and I is the current measured at E = 0.90 V vs RHE. The E-versus-log|I_k| curves or Tafel plots for the ORR normalized to each RDE electrode's respective Pt loading (i.e., mass-specific activity) are shown as insets in Figure 9. The Tafel plots shown in Figure 9 can be fitted to two Tafel regions at low- and high-current density regions (lcd and hcd, respectively). The two slopes are attributed to the change in the adsorption mode of the reaction intermediate from Temkin to Langmuirian types or a change in the surface coverage by −OH, which influences the adsorption of O_2.[23] The Tafel slopes for all eight electrocatalyst samples, both pre- and post-heat-treated, are well-defined at −53 mV dec^{-1} for the lcd region and −95 mV dec^{-1} for the hcd regions (E < 0.86 V), which indicates that the presence of any additives (PPA, $TaOPO_4$, Ta_2O_5) does not change the limiting step in the ORR mechanism on the Pt NPs. The observed Tafel slopes are also in good agreement with the Tafel slope reported in the literature for polycrystalline Pt,[23a,b] carbon-supported Pt electrocatalysts,[24] and TaO_x-capped Pt electrocatalysts.[21a] The Tafel plots in Figure 9 show that the ORR catalytic activity for the Pt/VC standard and Pt/[PPA/VC], e.g., the two samples in which the Pt particles are not "glued" to the VC surface by the

DOI: 10.1021/cs501791z
ACS Catal. 2015, 5, 3662–3674

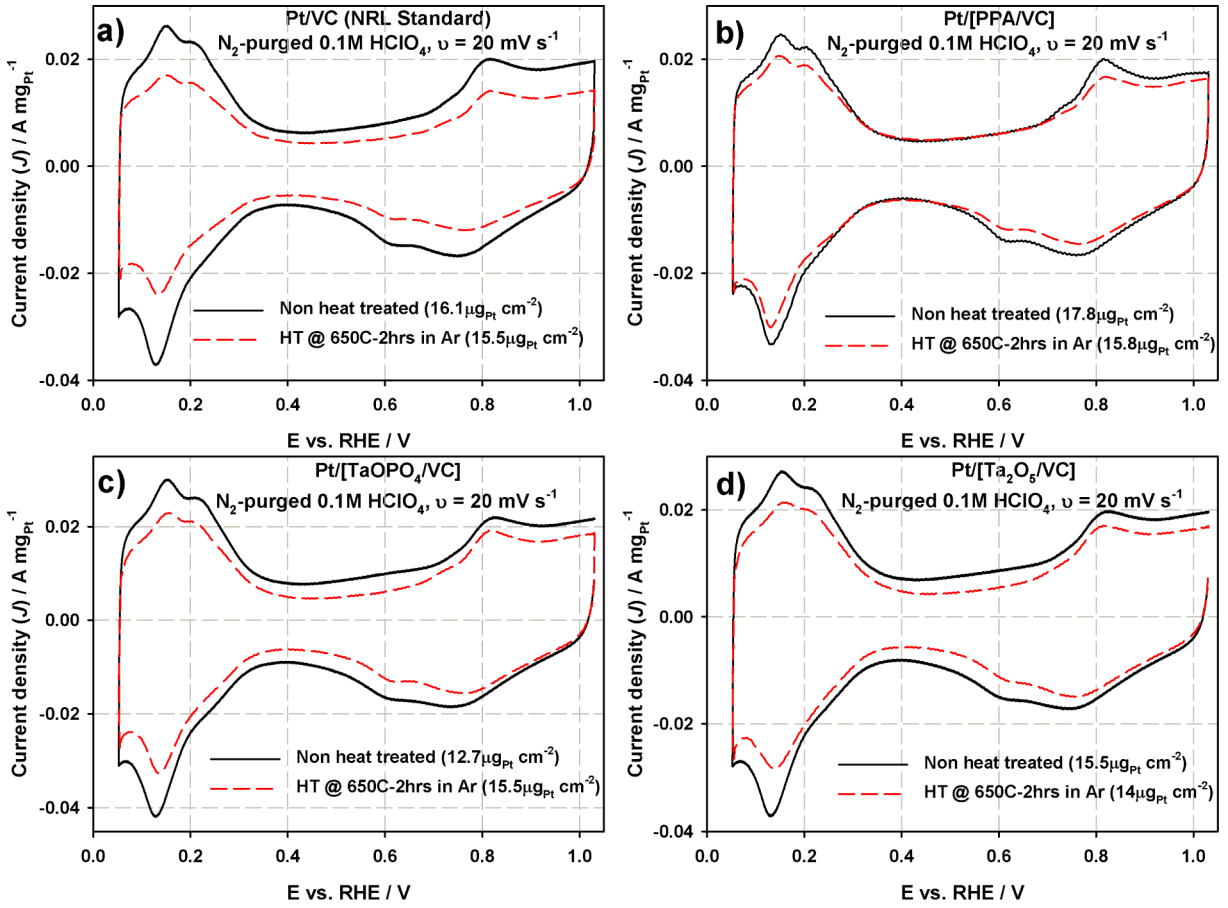

Figure 8. Cyclic voltammograms (CVs) recorded for the NHT and HT (a) Pt/VC control, (b) Pt/[PPA/VC], (c) Pt/Ta-[PPA/VC], and (d) Pt/[Ta_2O_5/VC] electrocatalysts in N_2-purged 0.10 M $HClO_4$ electrolyte. Cell temperature, 30 °C; potential scan rate, 20 mV s^{-1}.

Ta adhesive films, decreased after heat treatment, whereas the Pt/[$TaOPO_4$/VC] and Pt/[Ta_2O_5/VC] samples, for example, with adhesive Ta films, became more active after heat treatment.

The average values obtained for the Pt ECSA, Pt MA, and SA calculated at E = 0.90 V vs RHE for seven independent RDE thin-film electrodes for each of the electrocatalysts (both NHT and HT) are summarized in the histograms in Figure 10. The error bars correspond to the standard deviation for the seven independent measurements. The MAs and SAs are estimated by the calculation of I_k (using eq 2) and normalized to the Pt loading of the RDE electrode and the estimated Pt ECSA, respectively. The Pt ECSA of the different electrocatalysts estimated using eq 1 from the charge in the hydrogen adsorption potential region (i.e., 0.40−0.05 V vs RHE) are presented in Figure 10a, with the respective average Pt ECSA values (the error bars correspond to the standard deviation for the seven independent CV measurements). The average Pt ECSA values measured for the Pt/VC control, Pt/[PPA/VC], Pt/[$TaOPO_4$/VC], and Pt/[Ta_2O_5/VC] electrocatalysts before heat treatment are 97 ± 3, 93 ± 2, 115 ± 5, and 105 ± 4 m^2 g_{Pt}^{-1}, respectively. The average Pt ECSA values measured for the same electrocatalysts after heat treatment are 60 ± 3, 72 ± 2, 88 ± 5, and 85 ± 2 m^2 g_{Pt}^{-1}, respectively.

The general trend of ECSA loss with catalyst heat treatment is not surprising, as Pt NP coarsening is expected. In addition, not surprising is the 38% loss in ECSA for the Pt/VC control. The other three samples, Pt/[PPA/VC], Pt[$TaOPO_4$/VC], and Pt/[Ta_2O_5/VC], underwent a 22.6%, 23.5%, and 23.5% ECSA loss, respectively, which is expected for the Ta-containing samples that should presumably exhibit better adhesive properties, but is somewhat surprising for Pt[PPA/VC], which differed from the control only in having roughly 0.2 at. % P (based on XPS results). On the other hand, the SA for three of the four samples increased. For example, Pt/VC gained 47.8%, Pt/[Ta_2O_5/VC] gained 48.5%, and Pt[$TaOPO_4$/VC] gained an impressive 103%, more than doubling its SA, whereas Pt/[PPA/VC] actually lost 5.3%. The SA provides a more complete description as to why Pt/[PPA/VC], with the highest MA before heat treatment at 0.85 A mg_{Pt}^{-1}, essentially lost 27% of its MA, which is the product of the combined losses in both ECSA and SA. Any explanation as to why the PPA-treated sample has such a significant loss of its SA would be speculative; however, we would like to point out that this is yet another piece of evidence demonstrating the importance of the Ta atoms cross-linking the PPA in the Pt/[$TaOPO_4$/VC] sample. The Pt/VC control's MA stayed nearly the same, as the 38% loss in ECSA was offset by a 47.8% gain in SA. Pt/[Ta_2O_5/VC] had a 48.5% increase in SA that offset the 23.5% ECSA loss. Most impressive, however, is the large gain in SA for the $TaOPO_4$-treated sample, which after heat treatment exhibited a MA of 0.82 A mg_{Pt}^{-1}, a result that is surprising in light of the relatively unchanged XPS data for this sample. This demonstrates the significant improvement that the heat treatment procedure imparts on the $TaOPO_4$-treated catalyst. On the basis of the Ta XPS results, we speculate that the reduction of the Ta oxides in the Pt/[Ta_2O_5/VC] sample is the

DOI: 10.1021/cs501791z
ACS Catal. 2015, 5, 3662−3674

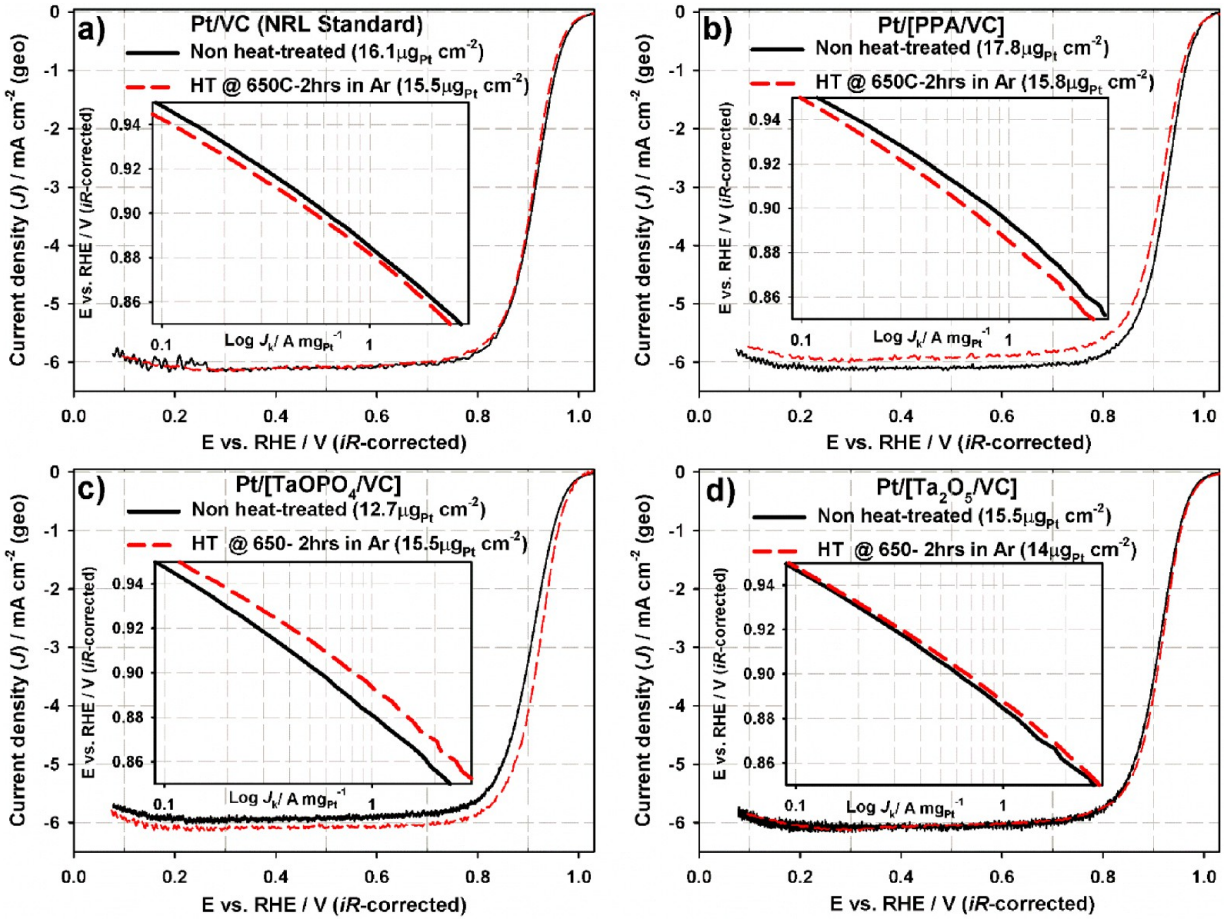

Figure 9. *iR* and background-corrected ORR polarization curves recorded at a potential scan rate of 20 mV s^{-1}, 1600 rpm, 30 °C in O_2-saturated 0.10 M $HClO_4$ for the NHT and HT (a) Pt/VC control, (b) Pt/[PPA/VC], (c) Pt/[$TaOPO_4$/VC], and (d) Pt/[Ta_2O_5/VC] electrocatalysts. Insets are the mass-transport-corrected Pt mass-based Tafel plots, which are plotted as a function of *iR*-corrected potential in the voltage range of 0.85−0.95 V.

main reason for a lower observed SA as compared with Pt[$TaOPO_4$/VC].

Electrocatalyst Durability Testing. To determine the stability of the electrocatalysts after heat treatment, durability tests were performed by continuous square potential cycling between 0.6 V vs RHE (30 s hold) and 1.2 V vs RHE (30 s hold) in N_2-purged 0.10 M $HClO_4$ for 1000 cycles. Figure 11 presents representative CVs (insets) and ORR polarization curves recorded before and after the durability test for the four heat-treated electrocatalyst samples (note that the ORR polarization curves shown in Figure 11 are only background-corrected). The electrode Pt loadings are also included (see inset Figure 11a−d) because they differ from those in Figure 9a. With repeated oxidation cycles, the CVs recorded for all the electrocatalysts exhibited a reduction in surface-area-dependent processes: the hydrogen adsorption/desorption region and the Pt−OH formation/reduction region, which are more pronounced for the Pt/VC-HT control and Pt/[PPA/VC]-HT electrocatalysts. Further, there is a positive shift of the onset potential of Pt−OH adsorption in the CVs recorded for both the Pt/VC-HT control and Pt/[PPA/VC]-HT electrocatalysts, indicative of a change (i.e., particle growth) in the electrocatalysts Pt particle size.

Sheng et al. have shown that with increasing Pt particle size, the onset potential of rising oxidation current and the peak voltage of the reduction peak are shifted positively.[25] For the Pt/VC-HT control (inset Figure 11a), the Pt ECSA value decreases from 60 before to 44 m^2 g_{Pt}^{-1} after 1000 oxidation cycles. Thus, 26% of the initial Pt ECSA is lost in the course of the durability test. Figure 11a also shows representative ORR polarization curves obtained for the Pt/VC-HT control electrode before and after the durability test. The Pt/VC-HT control electrode is not stable against the test, as indicated by the negative shift of the $E_{1/2}$ (from 920.4 to 908.5 mV). The MA value decreases from 0.55 to 0.37 A mg_{Pt}^{-1}, which translates into a loss of 33% from the initial ORR activity. A similarly significant decrease in the Pt ECSA is also observed for Pt/[PPA/VC]-HT, which decreased from 72 before to 48 m^2 g_{Pt}^{-1} after 1000 oxidation cycles, a 33% loss from the initial Pt ECSA during the durability test. The same trend was observed for the ORR activity of Pt/[PPA/VC]-HT, as the $E_{1/2}$ shifted from 917.7 to 906.4 mV, and the MA value decreased from 0.62 to 0.45 A mg_{Pt}^{-1}, a 27% loss in ORR activity. The observed decrease in the active surface area and the ORR catalytic activity for both the Pt/VC control and the Pt/[PPA/VC] samples are likely be predominantly caused by the coalescence of the Pt particles because it was shown by Sheng et al. that small Pt particles (∼2 nm) easily coalesce to form larger ones, which is consistent with particle migration and coalescence being a major catalyst degradation pathway.[25]

The histogram in Figure 11 displays the Pt ECSA and MA loss data for the electrocatalysts tested. Each bar represents the

DOI: 10.1021/cs501791z
ACS Catal. 2015, 5, 3662−3674

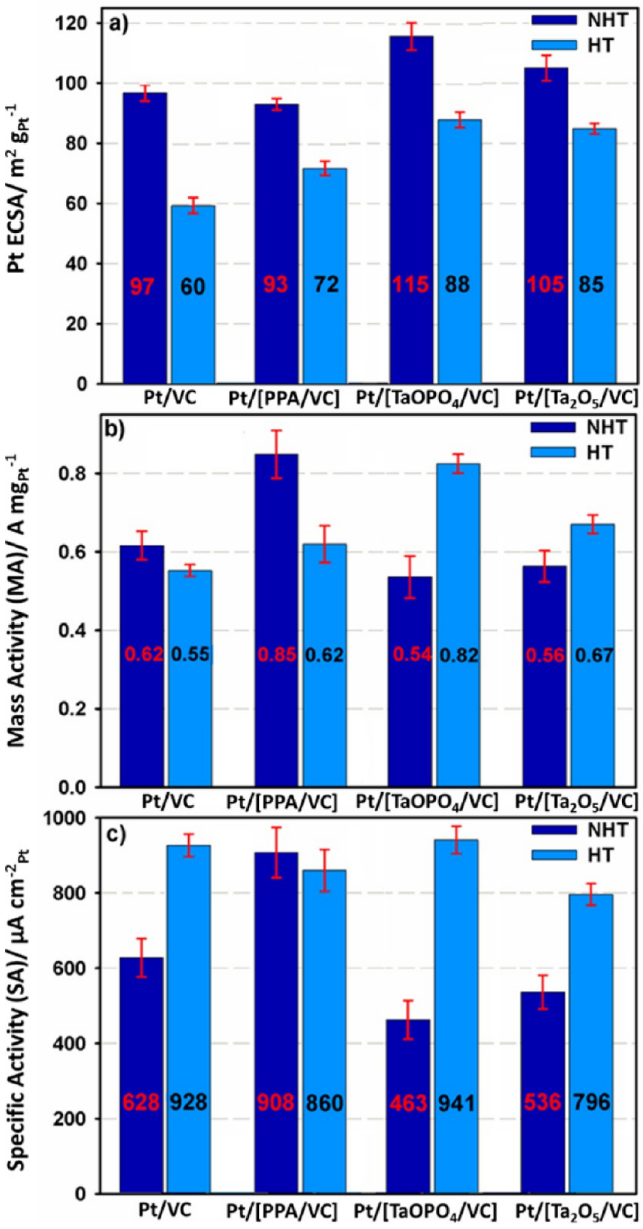

Figure 10. Estimated average (a) Pt ECSA, (b) MA, and (c) (SA) for the NHT and HT Pt/VC, Pt/[PPA/VC], Pt/[$TaOPO_4$/VC], and Pt/[Ta_2O_5/VC] electrocatalysts calculated at E = 0.90 V (iR corrected potential). Error bars represent the standard deviations obtained from seven independent measurements for each catalyst sample.

average value of three independent durability tests for each sample, and the error bar corresponds to the standard deviation for the three respective tests for each of the samples. The durability performance of the Pt/[$TaOPO_4$/VC]-HT and Pt/[Ta_2O_5/VC]-HT electrocatalysts (Figure 11c,d, respectively) was significantly better. The fresh Pt/[$TaOPO_4$/VC]-HT electrode showed an initial Pt ECSA of 88 $m^2g_{Pt}^{-1}$ and after 1000 oxidation cycles, the Pt ECSA value decreased to 70 $m^2g_{Pt}^{-1}$, which is a 20% loss in Pt ECSA. The fresh Pt/[Ta_2O_5/VC]-HT electrode showed an initial Pt ECSA of 85 $m^2g_{Pt}^{-1}$ and after 1000 oxidation cycles, the Pt ECSA value decreased to 75 $m^2g_{Pt}^{-1}$, or only a 12% loss in the Pt ECSA. Figure 11c,d also shows representative ORR polarization curves recorded for the Pt/[$TaOPO_4$/VC] and the Pt/[Ta_2O_5/VC] electrocatalysts before and after the durability test. After the durability test, $E_{1/2}$ is shifted by 7.9 and 2.4 mV for the Pt/[$TaOPO_4$/VC] and Pt/[Ta_2O_5/VC] electrocatalysts, respectively; and the MA values decreased from 0.74 to 0.59 A mg_{Pt}^{-1} for the Pt/[$TaOPO_4$/VC] electrocatalyst and from 0.55 to 0.49 A mg_{Pt}^{-1}, which are 20% and 11% decreases, respectively. The oxidation cycling durability test shows that both Pt/[$TaOPO_4$/VC] and Pt/[Ta_2O_5/VC] electrocatalysts are significantly more stable to oxidation cycling than the control Pt/VC and the Pt[PPA/VC] catalyst.

SUMMARY AND CONCLUSIONS

We have shown that the $TaOPO_4$ and Ta_2O_5 thin films likely act as adhesives, tethering the Pt NPs to VC supports, and a more concrete assessment of the role of polyphosphate and Ta on the activity and durability of ORR electrocatalysts can now be made. Our Pt-colloid based catalyst system has proven useful in eliminating unwanted variables and enabling the direct comparison of catalysts, with the primary variable being the various additives. A significant challenge in this work was to develop a set of samples that were as closely matched as possible. This was accomplished through the use of a colloid with a narrow particle size distribution as the source of the Pt NPs and using a low 10 wt % Pt loading to minimize particle growth during heat treatment. This approach resulted in four nearly perfectly matched catalyst samples with an almost identical Pt content, particle size distributions, and surface particle dispersion. The only variable remaining was the adhesive additive used for each sample, thereby allowing for a direct electrochemical comparison of the samples to determine the effects of each additive on the catalyst durability performance.

By creating a matched set of catalysts treated with the PPA, $TaOPO_4$, and Ta_2O_5 additives and a matching Pt/VC control, we were able to show a direct relationship of the higher electrocatalyst durability against voltage cycling correlated to the presence of the Ta-based adhesive films. The adhesive properties of the additives were indirectly evident from resistance to sintering during heating, the abnormal size distributions after heating for higher Pt loading samples, EDS elemental mapping, and colocation of Pt NPs with areas of Ta atoms corresponding to Ta-containing films on the VC surface. Electrocatalyst durability is significantly improved in the presence of the Ta-based adhesives, likely because of the elimination of the particle migration and coalescence catalyst degradation pathways. Our 10 wt % Pt[$TaOPO_4$/VC]-HT catalyst exhibited an impressive iR corrected MA of 0.82 A mg_{Pt}^{-1} in combination with a 33% improvement in durability over the Pt/VC control. This combination of high ORR activity and durability is particularly noteworthy. On the basis of the Ta XPS results, we speculate that the reduction of the Ta-oxides in the Pt/[Ta_2O_5/VC] sample producing a tantalum suboxide is an underlying reason for the observed lower SA as compared with Pt[$TaOPO_4$/VC], which had minimal Ta suboxide content after heat treatment. This was of particular significance because the Ta_2O_5 treated sample had 3× greater durability over the Pt/VC control (an 11% vs a 33% MA loss), whereas the $TaOPO_4$ treated sample had 1.7× better durability over the Pt/VC control (a 20% vs a 33% MA loss).

Our most important conclusion is that the two Ta-treated samples exhibited the best durability. We suggest that this is due to the Ta-based adhesives' immobilizing the Pt particles and minimizing the particle migration and coalescence catalyst

DOI: 10.1021/cs501791z
ACS Catal. 2015, 5, 3662−3674

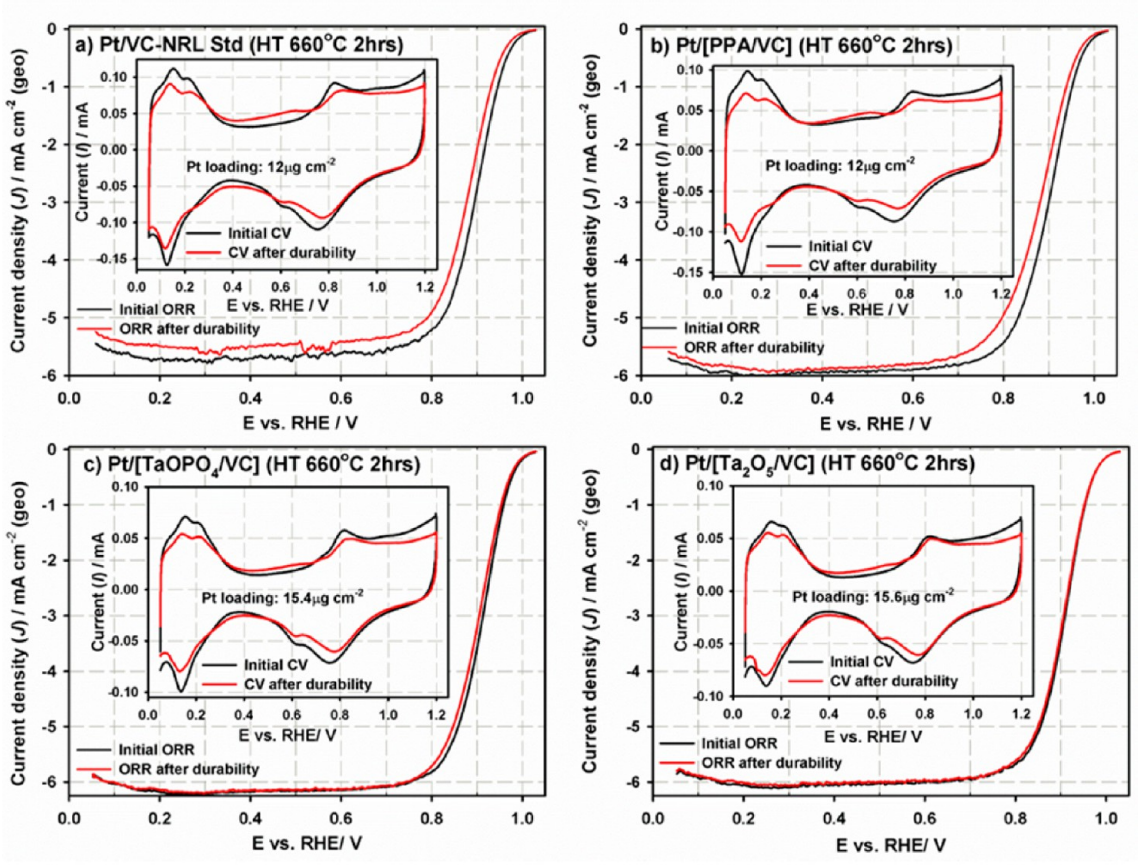

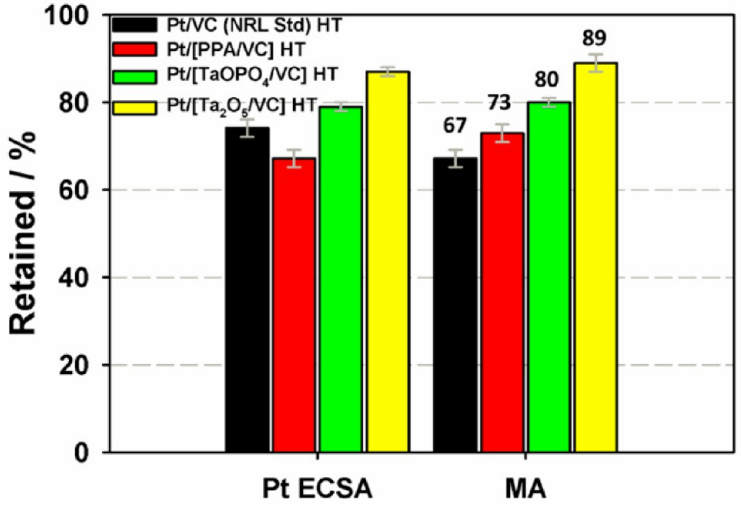

Figure 11. (a–d) Representative polarization curves recorded for O_2 reduction on (a) Pt/VC-HT control, (b) Pt/[PPA/VC]-HT, (c) Pt/[$TaOPO_4$/VC]-HT, and (d) Pt/[Ta_2O_5/VC]-HT electrocatalysts on a RDE before and after continuous square potential cycling between 0.6 V vs RHE (30 s hold) and 1.2 V vs RHE (30 s hold) in N_2-purged 0.10 M $HClO_4$ for a 1000 cycles. Potential scan rate, 20 mV s^{-1}; electrode rotation rate, 1600 rpm; electrolyte, O_2-saturated 0.10 M $HClO_4$; cell temperature, 30 °C. The insets show the CVs recorded for each respective electrocatalyst before and after the durability test. CVs recorded at a potential scan rate of 50 mV s^{-1} in N_2-purged 0.10 M $HClO_4$ electrolyte at 30 °C. Histogram: percentage of Pt ECSA and MA retained for the Pt/VC-HT control, Pt/[PPA/VC]-HT, Pt/[$TaOPO_4$/VC]-HT, and Pt/[Ta_2O_5/VC]-HT electrocatalysts when subjected to oxidation cycles. The bar represents the average value of three independent durability tests. The error bar corresponds to the standard deviation for the three durability tests performed for each sample.

degradation pathway, therefore making the catalyst more stable under voltage cycling conditions. Further studies of this catalyst system using direct in situ observation techniques, such as IL-TEM or IL-EELS tomography are warranted to better show the catalyst NP immobilization and will be pursued in the future. On the basis of this work, the concept of "gluing" catalyst NPs to graphitic supports is a generally applicable concept for electrocatalyst systems that require conductive graphitic

DOI: 10.1021/cs501791z
ACS Catal. 2015, 5, 3662–3674

supports and may be one way to resolve long-term durability problems for NP-based electrocatalysts supported on graphitic materials.

■ ASSOCIATED CONTENT

Supporting Information

The Supporting Information is available free of charge on the ACS Publications website at DOI: 10.1021/cs501791z.

Electrochemical experimental section, EDS elemental maping, representative TEM/STEM images used for particle size measurements, PXRD of the samples after heating, and XPS spectra of all electrocatalyst samples before and after heat treatment (PDF)

■ AUTHOR INFORMATION

Corresponding Author

*Address: Chemistry Division, Naval Research Laboratory, 4555 Overlook Ave., SW, Washington, D.C. 20375. Phone: 202-767-3130. Fax: 202-767-0594. E-mail: albert.epshteyn@nrl.navy.mil.

Notes

The authors declare no competing financial interest.

■ ACKNOWLEDGMENTS

The authors thank the Office of Naval Research for financial support. The authors thank Dr. Stephen Campbell (AFCC) and Dr. Jeremy J. Pietron (NRL) for technical discussions. Some of the TEM/STEM EDS elemental mapping and XPS analysis was conducted at ORNL's Center for Nanophase Materials Sciences, which is a U.S. Department of Energy, Office of Science User Facility.

■ REFERENCES

(1) Cao, A.; Lu, R.; Veser, G. *Phys. Chem. Chem. Phys.* **2010**, *12*, 13499−13510.

(2) Gasteiger, H. A.; Kocha, S. S.; Sompalli, B.; Wagner, F. T. *Appl. Catal., B* **2005**, *56*, 9−35.

(3) (a) Borup, R.; Meyers, J.; Pivovar, B.; Kim, Y. S.; Mukundan, R.; Garland, N.; Myers, D.; Wilson, M.; Garzon, F.; Wood, D.; Zelenay, P.; More, K.; Stroh, K.; Zawodzinski, T.; Boncella, J.; McGrath, J. E.; Inaba, M.; Miyatake, K.; Hori, M.; Ota, K.; Ogumi, Z.; Miyata, S.; Nishikata, A.; Siroma, Z.; Uchimoto, Y.; Yasuda, K.; Kimijima, K. I.; Iwashita, N. *Chem. Rev.* **2007**, *107*, 3904−3951. (b) Mathias, M. F.; Makharia, R.; Gasteiger, H. A.; Conley, J. J.; Fuller, T. J.; Gittleman, C. I.; Kocha, S. S.; Miller, D. P.; Mittelsteadt, C. K.; Xie, T.; Yan, S. G.; Yu, P. T. *Electrochem Soc. Interface* **2005**, *14*, 24−35.

(4) (a) Zhang, S. S.; Yuan, X. Z.; Hin, J. N. C.; Wang, H. J.; Friedrich, K. A.; Schulze, M. *J. Power Sources* **2009**, *194*, 588−600. (b) Shao-Horn, Y.; Sheng, W. C.; Chen, S.; Ferreira, P. J.; Holby, E. F.; Morgan, D. *Top. Catal.* **2007**, *46*, 285−305. (c) Tang, H.; Qi, Z. G.; Ramani, M.; Elter, J. F. *J. Power Sources* **2006**, *158*, 1306−1312.

(5) Gu, Y.; St-Pierre, J.; Joly, A.; Goeke, R.; Datye, A.; Atanassov, P. *J. Electrochem. Soc.* **2009**, *156*, B485−B492.

(6) (a) Mayrhofer, K. J. J.; Ashton, S. J.; Meier, J. C.; Wiberg, G. K. H.; Hanzlik, M.; Arenz, M. *J. Power Sources* **2008**, *185*, 734−739. (b) Meier, J. C.; Galeano, C.; Katsounaros, I.; Topalov, A. A.; Kostka, A.; Schuth, F.; Mayrhofer, K. J. J. *ACS Catal.* **2012**, *2*, 832−843. (c) Yu, Y. C.; Xin, H. L. L.; Hovden, R.; Wang, D. L.; Rus, E. D.; Mundy, J. A.; Muller, D. A.; Abruna, H. D. *Nano Lett.* **2012**, *12*, 4417−4423. (d) Schlogl, K.; Hanzlik, M.; Arenz, M. *J. Electrochem. Soc.* **2012**, *159*, B677−B682. (e) Perez-Alonso, F. J.; Elkjaer, C. F.; Shim, S. S.; Abrams, B. L.; Stephens, I. E. L.; Chorkendorff, I. *J. Power Sources* **2011**, *196*, 6085−6091. (f) Hartl, K.; Hanzlik, M.; Arenz, M. *Energy Environ. Sci.* **2011**, *4*, 234−238.

(7) Galeano, C.; Meier, J. C.; Peinecke, V.; Bongard, H.; Katsounaros, I.; Topalov, A. A.; Lu, A. H.; Mayrhofer, K. J. J.; Schuth, F. *J. Am. Chem. Soc.* **2012**, *134*, 20457−20465.

(8) Pylypenko, S.; Borisevich, A.; More, K. L.; Corpuz, A. R.; Holme, T.; Dameron, A. A.; Olson, T. S.; Dinh, H. N.; Gennette, T.; O'Hayre, R. *Energy Environ. Sci.* **2013**, *6*, 2957−2964.

(9) (a) Yoshii, K.; Tsuda, T.; Arimura, T.; Imanishi, A.; Torimoto, T.; Kuwabata, S. *RSC Adv.* **2012**, *2*, 8262−8264. (b) Takenaka, S.; Miyamoto, H.; Utsunomiya, Y.; Matsune, H.; Kishida, M. *J. Phys. Chem. C* **2013**, *118*, 774−783.

(10) Chen, S.; Wei, Z.; Qi, X.; Dong, L.; Guo, Y.-G.; Wan, L.; Shao, Z.; Li, L. *J. Am. Chem. Soc.* **2012**, *134*, 13252−13255.

(11) (a) Lightcap, I. V.; Kosel, T. H.; Kamat, P. V. *Nano Lett.* **2010**, *10*, 577−583. (b) Kamat, P. V. *J. Phys. Chem. Lett.* **2010**, *1*, 520−527.

(12) Garsany, Y.; Epshteyn, A.; Purdy, A. P.; More, K. L.; Swider-Lyons, K. E. *J. Phys. Chem. Lett.* **2010**, *1*, 1977−1981.

(13) Meier, J. C.; Galeano, C.; Katsounaros, I.; Witte, J.; Bongard, H. J.; Topalov, A. A.; Baldizzone, C.; Mezzavilla, S.; Schuth, F.; Mayrhofer, K. J. J. *Beilstein J. Nanotechnol.* **2014**, *5*, 44−67.

(14) Wang, Y.; Ren, J. W.; Deng, K.; Gui, L. L.; Tang, Y. Q. *Chem. Mater.* **2000**, *12*, 1622−1627.

(15) Korovina, A.; Garsany, Y.; Epshteyn, A.; Purdy, A. P.; More, K.; Swider-Lyons, K. E.; Ramaker, D. E. *J. Phys. Chem. C* **2012**, *116*, 18175−18183.

(16) (a) Garsany, Y.; Ge, J.; St-Pierre, J.; Rocheleau, R.; Swider-Lyons, K. E. *J. Electrochem. Soc.* **2014**, *161*, F628−F640. (b) Garsany, Y.; Singer, I. L.; Swider-Lyons, K. E. *J. Electroanal. Chem.* **2011**, *662*, 396−406. (c) Garsany, Y.; Baturina, O. A.; Swider-Lyons, K. E.; Kocha, S. S. *Anal. Chem.* **2010**, *82*, 6321−6328.

(17) Garsany, Y.; Epshteyn, A.; More, K. L.; Swider-Lyons, K. E. *ECS Electrochem. Lett.* **2013**, *2*, H46−H50.

(18) Swider, K. E.; Rolison, D. R. *J. Electrochem. Soc.* **1996**, *143*, 813−819.

(19) (a) NIST;. (b) Khanuja, M.; Sharma, H.; Mehta, B. R.; Shivaprasad, S. M. *J. Electron Spectrosc. Relat. Phenom.* **2009**, *169*, 41−45.

(20) Gregoire, J. M.; Tague, M. E.; Cahen, S.; Khan, S.; Abruna, H. D.; DiSalvo, F. J.; van Dover, R. B. *Chem. Mater.* **2010**, *22*, 1080−1087.

(21) (a) Awaludin, Z.; Moo, J. G. S.; Okajima, T.; Ohsaka, T. *J. Mater. Chem. A* **2013**, *1*, 14754−14765. (b) Garsany, Y.; Epshteyn, A.; Purdy, A. P.; More, K. L.; Swider-Lyons, K. E. *J. Phys. Chem. Lett.* **2010**, *1*, 1977−1981.

(22) (a) Mayrhofer, K. J. J.; Strmcnik, D.; Blizanac, B. B.; Stamenkovic, V.; Arenz, M.; Markovic, N. M. *Electrochim. Acta* **2008**, *53*, 3181−3188. (b) Markovic, N. M.; Gasteiger, H. A.; Ross, P. N. *J. Phys. Chem.* **1995**, *99*, 3411−3415.

(23) (a) Damjanov, A.; Brusic, V. *Electrochim. Acta* **1967**, *12*, 1171−1184. (b) Damjanov, A.; Brusic, V. *Electrochim. Acta* **1967**, *12*, 615−628. (c) Wang, J. X.; Markovic, N. M.; Adzic, R. R. *J. Phys. Chem. B* **2004**, *108*, 4127−4133.

(24) Paulus, U. A.; Wokaun, A.; Scherer, G. G.; Schmidt, T. J.; Stamenkovic, V.; Radmilovic, V.; Markovic, N. M.; Ross, P. N. *J. Phys. Chem. B* **2002**, *106*, 4181−4191.

(25) Sheng, W.; Chen, S.; Vescovo, E.; Shao-Horn, Y. *J. Electrochem. Soc.* **2011**, *159*, B96−B103.

DOI: 10.1021/cs501791z
ACS Catal. 2015, 5, 3662−3674